# Computation of inductively coupled air plasma flow in the torches

# Computation of inductively coupled air plasma flow in the torches

**S A Vasilevskii, A F Kolesnikov, A I Bryzgalov, S E Yakush**

Ishlinsky Institute for Problems in Mechanics RAS, Prospekt Vernadskogo 101-1, Moscow, 119526, Russia

vasil_ipmech@mail.ru

**Abstract**. Software was developed to calculate electric field amplitude in the induction plasmatron discharge channel in framework of 2D model with far field boundary conditions. This code was integrated with the solver for Navier-Stokes equations for plasma flow in the plasmatron channel. Numerical simulation of inductively coupled plasma flow was carried out for the channels of IPG-4 and IPG-3 induction plasmatrons operating in IPMech RAS. Computations were performed twice: first, the electric field amplitude was calculated with the more accurate 2D model, next - with the simplified 1D model to provide detailed compare of the accuracy of results obtained with use of 1D model. The gas-dynamic parameters (flow velocity, temperature) at the exit section of the channels obtained with 1D model are within the error from 0.4% to 4% for IPG-4 plasmatron; the corresponding error for IPG-3 plasmatron is 16% to 26%. Numerical simulation results for IPG-3 plasmatron are presented for the first time.

## 1. Introduction

Inductively coupled plasma (ICP) flow is one of the important objects for numerical simulation from the viewpoint of various applications and studying fundamental physical processes. A modern direction of induction plasma application is simulation of dissociated gas flow thermochemical action on a surface of thermal protection material and investigation of the materials surface catalycity [1]. Two induction plasmatrons, IPG-4 and IPG-3, are available in the Institute for Problems in Mechanics (IPMech RAS), they are used intensively for studying physical processes in high-enthalpy jets generated by induction plasmatrons and for material testing in such jets. The plasmatrons, experimental techniques and CFD codes developed for complex investigation of heat transfer from the jet to testing materials and for determination of material surface catalytic properties with respect to atoms recombination are described in [2–6].

Numerical simulation of ICP flow in a plasmatron discharge channel is a complicated problem even for the case of equilibrium plasma flow due to the large flow vortices that are formed after the inlet section. The room temperature gas inflows in the channel through a narrow (2-3 mm) inlet slot with a swirl angle β of about 45° to provide flow swirling, $\tan(\beta) = W/U$, $U$ and $W$ are the axial and tangential velocity components. The inductor coil with a high radio-frequency (RF) current encircles the channel and provides powerful electromagnetic field within the inductor region of the channel. The Joule heat production and Lorentz force lead to the strong plasma heating and so called "magnetic pressure" that affects the complicated flow structure with primary and secondary vortices.

Calculation of electromagnetic field within the channel is important part of the total problem of ICP numerical simulation. The more accurate 2D model for electromagnetic field was used in [7]; it requires the use of extended computational grid for electromagnetic field calculation to apply the far field boundary conditions - electromagnetic field turns to zero at far boundaries. The simplified 1D model was first proposed [8] and then used for ICP numerical simulation for IPG-4 [4-6]; it allows to save CPU time and programming efforts. The detailed comparison with the code developed in von Karman Institute for Fluid Dynamics confirmed the good accuracy of this 1D model for argon plasma flow in IPG-4 channel [9]. In this paper we provide detailed comparison of 2D and 1D models for electromagnetic field for ICP calculations in IPG-4 and IPG-3 plasmatrons for air plasma. The configuration of discharge channels for both plasmatrons is a simple cylinder; the air flow in the channels is always subsonic. Note that numerical simulation results for IPG-3 plasmatron are presented here for the first time.

## 2. Problem formulation

ICP flow in the plasmatron discharge channel is calculated on the basis of Navier-Stokes gas-dynamic equations coupled with the simplified Maxwell equation for the electric field amplitude. The following assumptions are used for the gas-dynamic part: the subsonic flow is stationary, laminar, equilibrium, and axisymmetric, with a swirl in azimuthal direction. High frequency electromagnetic field does not influence on transport properties of plasma, radiative processes are negligible. The air flow can be considered as equilibrium at sufficiently large pressure P≥0.05 atm, and radiative processes are not very essential for sufficiently low plasmatron power, i.e. sufficiently low flow temperature [10].

The governing equations are two-dimensional Navier-Stokes equations with three velocity components - axial, radial and tangential component due to the flow spinning. The equations are written in the cylindrical coordinate system, they include source terms corresponding to the electromagnetic field influence: $F_z$, $F_r$ are axial and radial components of the Lorentz force (the so called magnetic pressure); $Q_J$ is Joule heat production [5]. These source terms are expressed by the electric field amplitude and will be written below.

Boundary conditions for the gas-dynamic equations are as follows. The necessary flow parameters including velocity tangential component are specified at the annular inlet slot at the channel entry section. Zero values for velocity components and certain values of temperature are prescribed at all solid surfaces (the channel wall, the face of the gas injector interface). Symmetry conditions are applied at the channel axis. The so-called “soft” boundary conditions are applied at the channel exit section, i.e. the unknown functions are assumed to be constant near this boundary.

RF electric current oscillating in the inductor coil produces a vortical electric field within the discharge channel. The inductor coil is treated as a number of separate turns with the same current in each of them. Inductor turns are represented as thin equidistant rings perpendicular to the symmetry axis. Navier-Stokes equations including the source terms are assumed to be time-averaged with respect to RF electric field oscillations. The electromagnetic field is treated as monochromatic one with use of complex amplitudes for electric and magnetic fields:

$$\vec{E}(t,z,r) = \vec{E}(z,r)\cdot exp(-i\omega t), \quad \vec{H}(t,z,r) = \vec{H}(z,r)\cdot exp(-i\omega t)$$

here $z$, $r$ are the axial and radial coordinates, $t$ is the time, $\omega = 2\pi f$ - circular frequency, $f$ - frequency of the inductor current. For the experimental conditions in IPG-4, IPG-3 plasmatrons the following assumptions can be applied [11]: $\omega << \nu_e$ and $|\varepsilon| << 4\pi\sigma/\omega$, here $\nu_e$ is the electron collisions frequency, $\varepsilon$ - dielectric permittivity of plasma. The last inequality means that the displacement current is negligible. Also, the following common assumptions are used: plasma is quasi-neutral; plasma magnetic permeance $\mu = 1$, and dielectric constant does not depend on electromagnetic field and so does not depend on $z$ and $r$.

*2.1. 2D formulation for the electric field amplitude equation*

In frameworks of the above assumptions, Maxwell equations with use of Ohm's law and symmetry conditions lead to the following equations for tangential $E_\theta(z,r)$, axial $E_z$ and radial $E_r$ components of the electric field amplitude:

$$\frac{\partial^2 E_\theta}{\partial z^2} + \frac{\partial}{\partial r}\left(\frac{1}{r}\frac{\partial}{\partial r} r E_\theta\right) = -i\omega\mu_0\sigma E_\theta, \quad E_z = 0, \; E_r = 0 \tag{1}$$

here $\mu_0$ is vacuum magnetic permeance, $\sigma$ is the plasma electric conductivity. The two-dimensional (2D) elliptic equation (1) for the tangential component of the electric field amplitude $E_\theta(z,r)$ is solved on far-field mesh, extended beyond the channel, to allow the use of the simple far-field boundary conditions:

$$E_\theta(z, r = \pm\infty)=0; \; E_\theta(z = \pm\infty, r)=0 \tag{2}$$

In addition, the symmetry condition $E_\theta(z, r=0) = 0$ is used also.

Following [7], to avoid singularities near the coil rings, the total field amplitude $E_\theta$ is split to a singular part $E_{\theta V}$ induced by the outer inductor rings and a nonsingular plasma-induced part $E_{P\theta}$:

$$E_\theta = E_{V\theta} + E_{P\theta} \tag{3}$$

The equation (1) for $E_\theta$ then can be rewritten so:

$$\frac{\partial^2 E_{P\theta}}{\partial z^2} + \frac{\partial}{\partial r}\left(\frac{1}{r}\frac{\partial}{\partial r} r E_{P\theta}\right) = -i\omega\mu_0\sigma( E_{V\theta} + E_{P\theta} ) \tag{4}$$

Analytical formula for the electric field induced by a single thin current-carrying loop can be found in [12]. The vacuum-field amplitude $E_{V\theta}$ is then calculated by adding up contributions of the discrete coil rings of inductor. Singularities in $E_{V\theta}$ near the coil rings do not affect the equation (4) because the electrical conductivity $\sigma$ is zero outside the channel.

The far-field boundary conditions can be rewritten so:

$$E_{P\theta}(z, r = \pm\infty)=0; \; E_{P\theta}(z = \pm\infty, r)=0 \tag{5}$$

*2.2. 1D formulation for the electric field amplitude equation*

Solution of 2D equation (4) requires additional computer time and efforts to solve elliptic equation on far-field mesh. To save time, the simplified 1D model for the electric field was proposed based on the assumption [8]: $\partial E_\theta / \partial z << \partial E_\theta / \partial r$. This assumption seems to be reasonable for the relatively thin plasmatron discharge channel (channel radius $R_c$ is about 10 times smaller than its length). With use of this assumption, equation (1) can be simplified to the ordinary differential equation:

$$\frac{d}{dr}\left(\frac{1}{r}\frac{d}{dr} r E_\theta\right) = -i\omega\mu_0\sigma E_\theta \tag{6}$$

Boundary condition for this equation is $E_\theta(z, r=0) = 0$ at the symmetry axis and the following approximate condition at the channel wall [5]:

$$r = R_c: \quad \frac{1}{r}\frac{d}{dr}(r E_\theta) = i\omega\mu_0 H_{Vz}(z) \tag{7}$$

Here $H_{Vz}$ is the vacuum-part of axial component of the magnetic field amplitude at the channel wall, produced only by the outer inductor rings. If we replace $H_{Vz}$ by the total value $H_z = H_{Pz} + H_{Vz}$, then equation (7) will be accurate, but the value $H_{Pz}$ is not known before the solution of the problem, so we have to assume that $H_{Vz}$ could stand for $H_z$ in the condition (7), e.g. for small plasmatron power regimes.

As a result, we obtain a quasi-one-dimensional formulation (6), (7) for the solution of electrodynamic part of the problem, here $E_\theta$ depends on $z$ due to the boundary condition only. Note, that in 1D case the magnetic field amplitude has only axial non-zero component $H_z$, and $F_r$=0.

*2.3. Source terms*

Time-averaged source terms for the time-averaged Navier-Stokes equations are the axial and radial components of Lorentz force $F_z$, $F_r$ (so called magnetic pressure) and Joule heat production $Q_J$. They are expressed via $E_\theta$ (here and further $E_\theta = E_{V\theta} + E_{P\theta}$):

$$F_z = -\frac{\sigma}{2\omega} Re\left\{E_\theta\left(i\frac{\partial E_\theta}{\partial z}\right)^*\right\}, \quad F_r = -\frac{\sigma}{2\omega}\frac{1}{r} Re\left\{E_\theta\left(i\frac{\partial rE_\theta}{\partial r}\right)^*\right\}, \quad Q_J = \frac{\sigma}{2} E_\theta E_\theta^*$$

here Re means the real part of a complex value, asterisk is the conjugation sign for a complex value.

## 3. Numerical solution techniques

Numerical solution of the 2D Navier-Stokes equations is achieved by the finite-volume method on the staggered grid within the channel region. The grid is non-uniform rectangular one both in axial (103 nodes) and radial (93 nodes) directions. The grid is refined in the radial direction near the torch wall; the grid is refined in the axial direction near the torch inlet section and within the inductor region.

Value of the inductor current amplitude $I_0$ is determined in process of iterations by the prescribed value of power input in plasma $N_{pl}$. As to a value of $N_{pl}$ itself, it should be specified by both the measured value of anode power $N_{ap}$ and the plasmatron efficiency $\eta_{eff}$ obtained from special experimental measurements: $N_{pl} = \eta_{eff} \cdot N_{ap}$. So, to determine the $I_0$ at each iteration we first calculate the electric field assuming that the inductor current amplitude equals to unit ($I_1$=1), and then integrate Joule heat production inputs from all the computation cells to obtain the total computational $Q_{Jcomp}$ and the relation of the specified $N_{pl}$ and $Q_{Jcomp}$: $\alpha = N_{pl} / Q_{Jcomp}$, and then we rescale the inductor current amplitude: $I_0 = \sqrt{\alpha}$. The necessary transport coefficients (including electrical conductivity) and thermodymamic properties are determined simultaneously in process of numerical simulation for each flow point by a rather accurate interpolation across the previously calculated tables. Such tables for equilibrium air mixture have been calculated as functions of pressure and temperature in advance in the temperature and pressure regions $300 \le T \le 20000$ K, $0.001 \le P \le 10$ atm. The calculation of transport coefficients for the tables were made with use of accurate formulas of Chapman-Enskog method [13-15] for the second and third non-zero approximation numbers, i.e. the numbers of terms in Sonine polynomials expansions of Boltzmann's equation solution that provide a good convergence. The reliable data on the interaction potentials and collision integrals were used for all pairs of particles [16]. The 22 components were accounted for the dissociated partially ionized air mixture including some second ions.

*3.1. Numerical solution of Navier-Stokes equations*

Navier-Stokes equations solution technique is based on the control volumes method and SIMPLE algorithm of Patankar and Spalding with use of the staggered grid [17]. Convective terms are approximated by the finite differences with the first order accuracy to provide better monotonicity property. Modifications of the Patankar & Spalding method were made to provide the convergence of iterations for a complicated ICP flow with large vortices. In particular, the unknown functions are determined with use of additional under-relaxation procedure to increase stability of the solution technique.

*3.2. Computation of electric field amplitude with 1D model*

Thomas algorithm ("sweep") for 3-diagonal matrix equations with use of complex variables is applied to solve the boundary value problem (6)-(7) to obtain the complex value of electric field amplitude tangential component $E_\theta$ and magnetic field amplitude axial component $H_z$.

### *3.3. Computation of electric field amplitude with 2D model*

The two-dimensional boundary-value problem described by the equations (4)–(5) was solved numerically in a domain which was extended beyond the induction channel, so that the far-field boundary conditions (5) could be applied. The electric field was decomposed into two components described by (3), and the actual approximation according to (4) was performed for the electric field induced by plasma, $E_{P\theta}$.

The elliptic operator on the left-hand side of (4) was approximated by the standard second-order scheme applied to the real and imaginary parts of the electric field. In (4), the same operator applies to both the real-valued and imaginary parts, coupling between these occurs on the right-hand side. The resulting system of algebraic equations with sparse matrix was solved iteratively by an efficient ILUT-preconditioned GMRES method [18] implemented in SPARSKIT numerical package [19].

## 4. Results and discussion

Computations were made for the experimental regimes of the two IPMech RAS facilities - induction plasma generators IPG-4 and IPG-3 at the single pressure value $P$=100 mbar.

IPG-4 plasmatron parameters are as follows: the inductor current frequency $f$=1.76 MHz, the discharge channel length $L_c$=400 mm, the discharge channel diameter $D_c$= 80 mm. IPG-3 parameters are as follows: $f$= 0.44 MHz, $L_c$= 870 mm, $D_c$=192 mm. For each plasmatron the computations were made for three values of power. Each computation was made twice, with use of 1D and 2D models for calculation of electric field. The same gas-dynamic solver was used for all cases. The main goal of this work was detailed comparison of 1D and 2D models for electric field calculation for the two plasmatrons for different power regimes. The basic results of comparison of the 1D and 2D calculations are presented in the tables 1 and 2 for IPG-4 and IPG-3 plasmatrons.

**Table 1.** Comparison of 1D and 2D calculations for IPG-4.

| $N_{ap}$ | $N_{pl}$ | $U_c$, m/s | | | $h_c$, MJ/kg | | | $T_c$, K | | | $I_0$, A | | |
|---|---|---|---|---|---|---|---|---|---|---|---|---|---|
| kW | kW | 1D | 2D | % | 1D | 2D | % | 1D | 2D | % | 1D | 2D | % |
| 70 | 44 | 220 | 228 | *4* | 49.7 | 51.3 | *3* | 9539 | 9735 | *2* | 373 | 367 | *2* |
| 45 | 29 | 155 | 157 | *1* | 36.5 | 37.8 | *3* | 7032 | 7223 | *3* | 317 | 320 | *1* |
| 20 | 12 | 69.0 | 69.3 | *0.4* | 17.6 | 17.9 | *2* | 5672 | 5691 | *0.3* | 312 | 310 | *0.6* |

The notations in the tables 1 and 2 are as follows: $N_{ap}$ and $N_{pl}$ are the plasmatron anode power and power input in plasma; $U_c$, $h_c$, $T_c$ are plasma velocity, enthalpy and temperature at the symmetry axis at the channel exit section; $I_0$ is the amplitude of the inductor current. The sub-columns 1D and 2D correspond to the parameters calculated with use of 1D and 2D models for electric field amplitude. The sub-column % corresponds to the percent difference of the parameters calculated with use of 1D and 2D models.

**Table 2.** Comparison of 1D and 2D calculations for IPG-3.

| $N_{ap}$ | $N_{pl}$ | $U_c$, m/s | | | $h_c$, MJ/kg | | | $T_c$, K | | | $I_0$, A | | |
|---|---|---|---|---|---|---|---|---|---|---|---|---|---|
| kW | kW | 1D | 2D | % | 1D | 2D | % | 1D | 2D | % | 1D | 2D | % |
| 400 | 240 | 219 | 261 | *16* | 55.3 | 67.1 | *18* | 10148 | 11014 | *8* | 899 | 1126 | *20* |
| 300 | 180 | 170 | 213 | *20* | 51.4 | 62.0 | *17* | 9745 | 10674 | *9* | 775 | 1010 | *23* |
| 200 | 120 | 107 | 145 | *26* | 44.0 | 52.7 | *17* | 8531 | 9896 | *14* | 637 | 856 | *26* |

It is clear from tables 1, 2 that for IPG-4 plasmatron the use of 1D model to calculate the electric field amplitude provides good (for low power) or satisfactory (for high power) results for the gas-dynamic parameters at the channel exit section. But for the IPG-3 facility the use of 1D model leads to essential errors even in the gas-dynamic parameters at the channel exit section.

The detailed comparison of the results obtained with use of 1D and 2D models is presented in the Figures below. The contours of dimensionless stream function (f), isotherms (T), contours of the electric and magnetic field amplitudes ($E_\theta$, $H_z$), calculated with use of 1D and 2D models, are presented in figures 1– 4 for IPG–4 for $P$=100 mbar, $N_{ap}$= 45 kW, $N_{pl}$=29 kW.

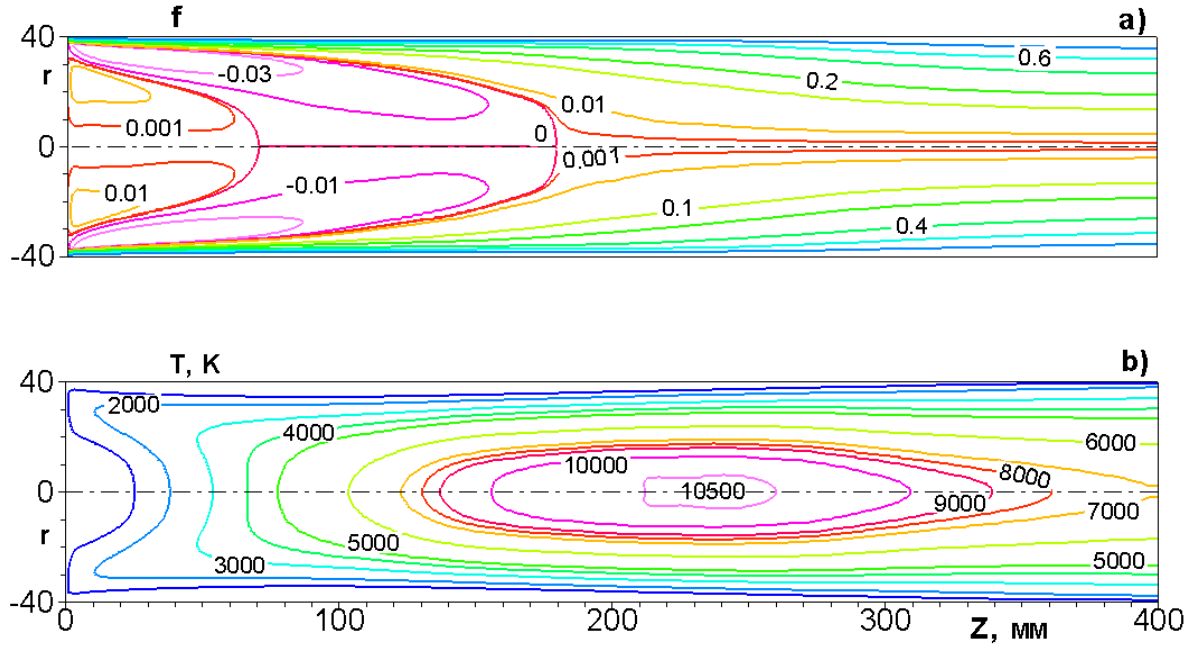


**Figure 1.** Contours of dimensionless stream function (a) and isotherms (b) in IPG–4 discharge channel calculated with use of 1D model for the electric field amplitude.

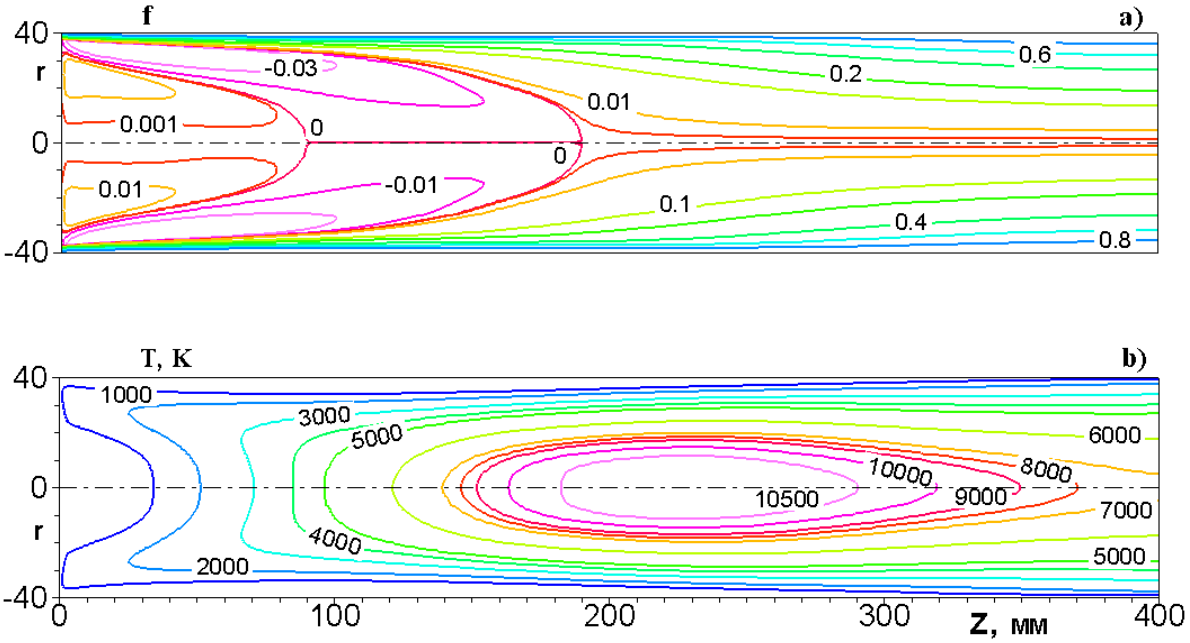


**Figure 2.** Contours of dimensionless stream function (a) and isotherms (b) in IPG–4 discharge channel calculated with use of 2D model for the electric field amplitude.

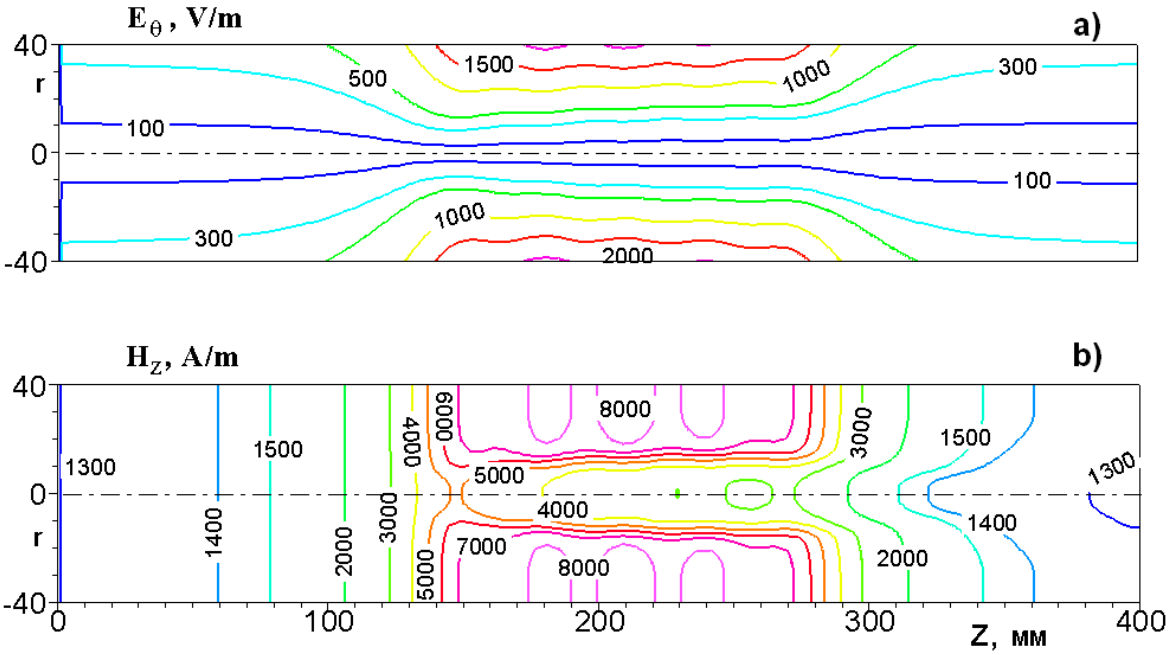


**Figure 3.** Contours of the amplitudes of electric field (a) and magnetic field (b) in IPG-4 discharge channel calculated with use of 1D model.

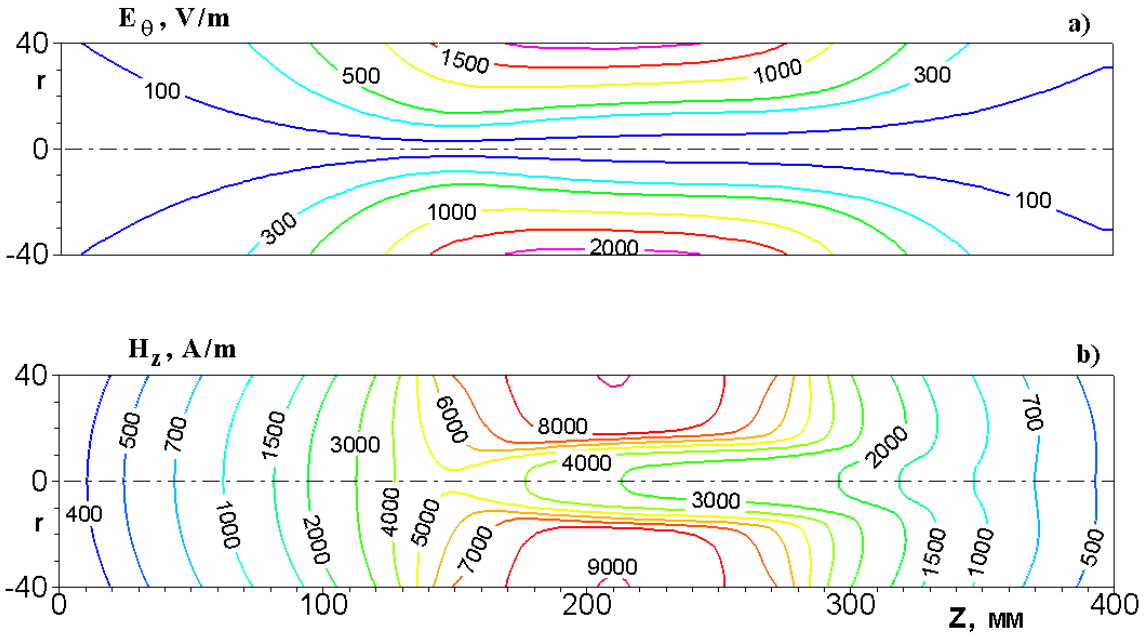


**Figure 4.** Contours of the amplitudes of electric field (a) and magnetic field (b) in IPG-4 discharge channel calculated with use of 2D model.

It is clear from the comparison of Figures 1 and 2, that the flow structures calculated with use of 1D and 2D models are similar, but slightly different, e.g. the length of secondary vortex near the inflow interface is greater for 2D case; the temperature maximums are nearly the same for 1D and 2D cases, but the geometry of isotherms is slightly different. The comparison of figures 3 and 4 shows that the maximum values of electric and magnetic field amplitudes within the inductor region are nearly the same for 1D and 2D cases, but the geometry of the contours is different.

The contours of dimensionless stream function, isotherms, electric and magnetic field amplitudes, calculated with use of 1D and 2D models, are presented in the figures 5–8 for IPG-3 for $P = 100$ mbar, $N_{ap}$=300 kW, $N_{pl}$=180 kW.

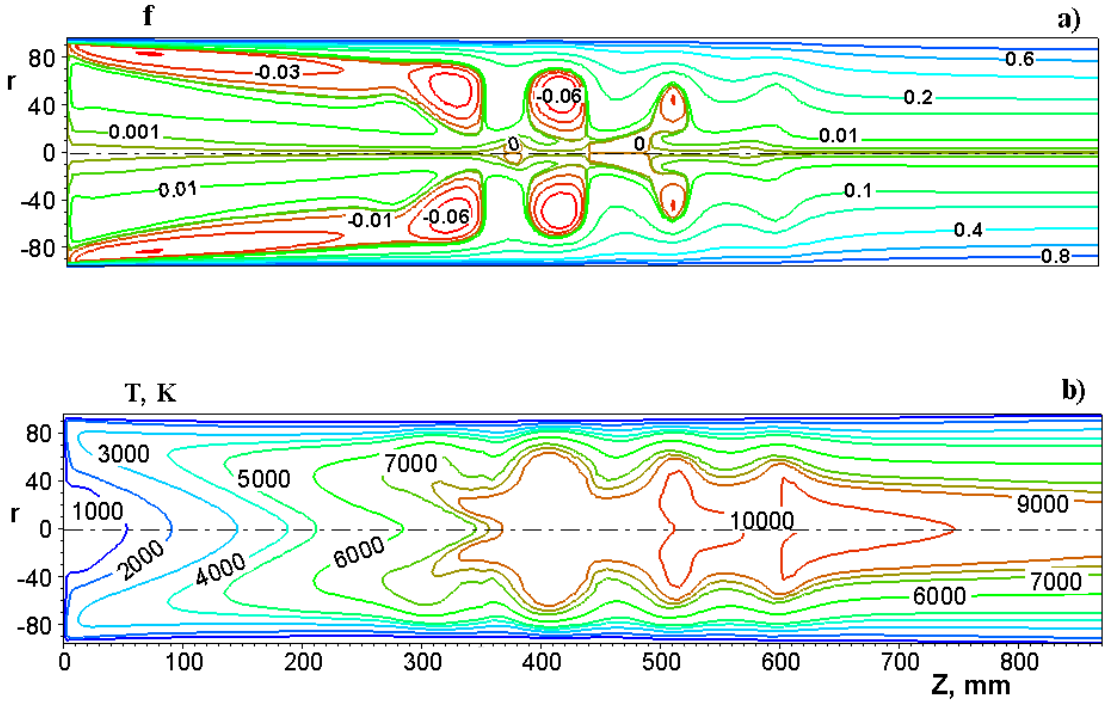


**Figure 5.** Contours of dimensionless stream function (a) and isotherms (b) in IPG-3 discharge channel calculated with use of 1D model for the electric field amplitude.

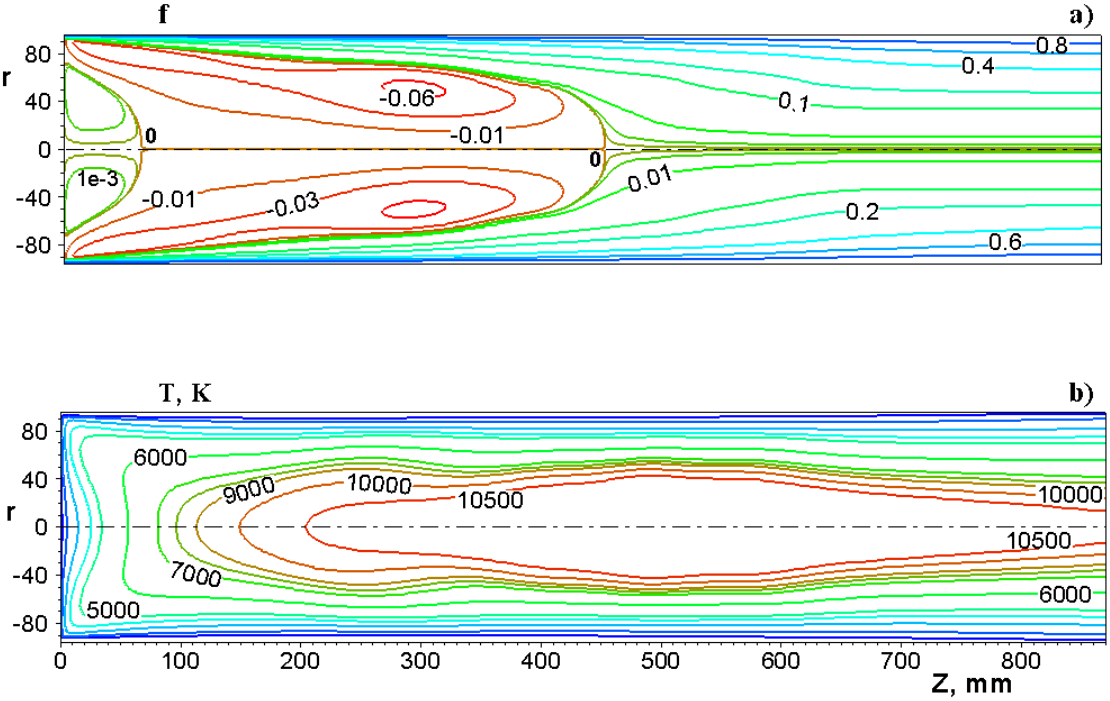


**Figure 6.** Contours of dimensionless stream function (a) and isotherms (b) in IPG-3 discharge channel calculated with use of 2D model for the electric field amplitude.

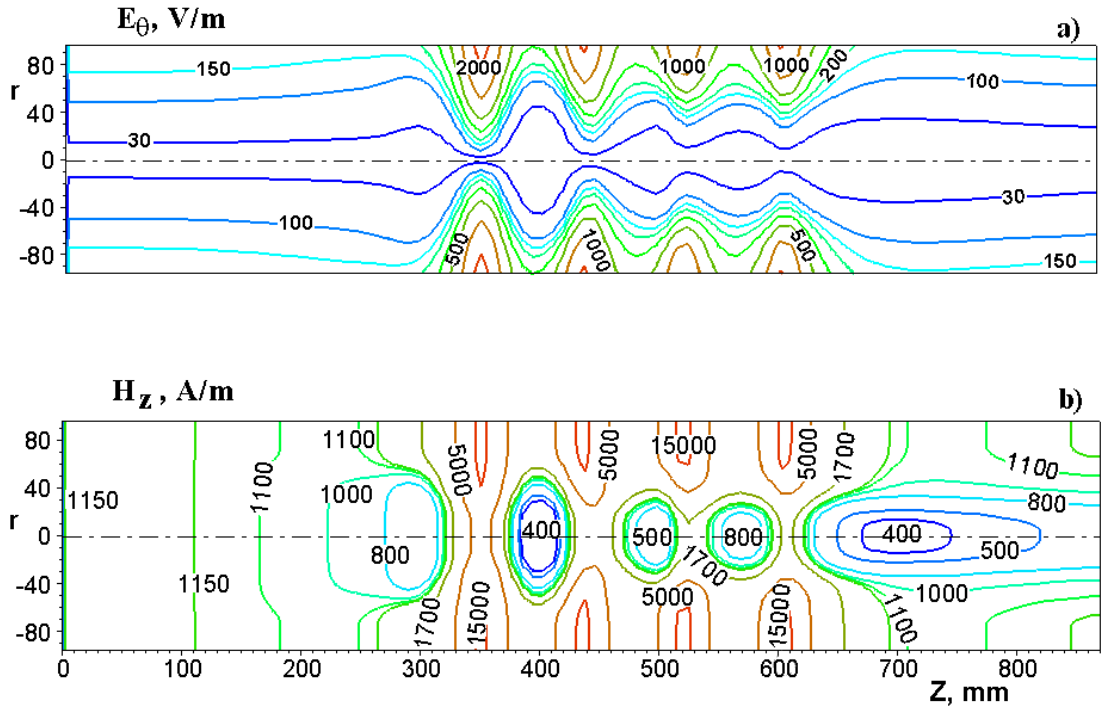


**Figure 7.** Contours of electric field (a) and magnetic field (b) amplitudes in IPG-3 channel, 1D model.

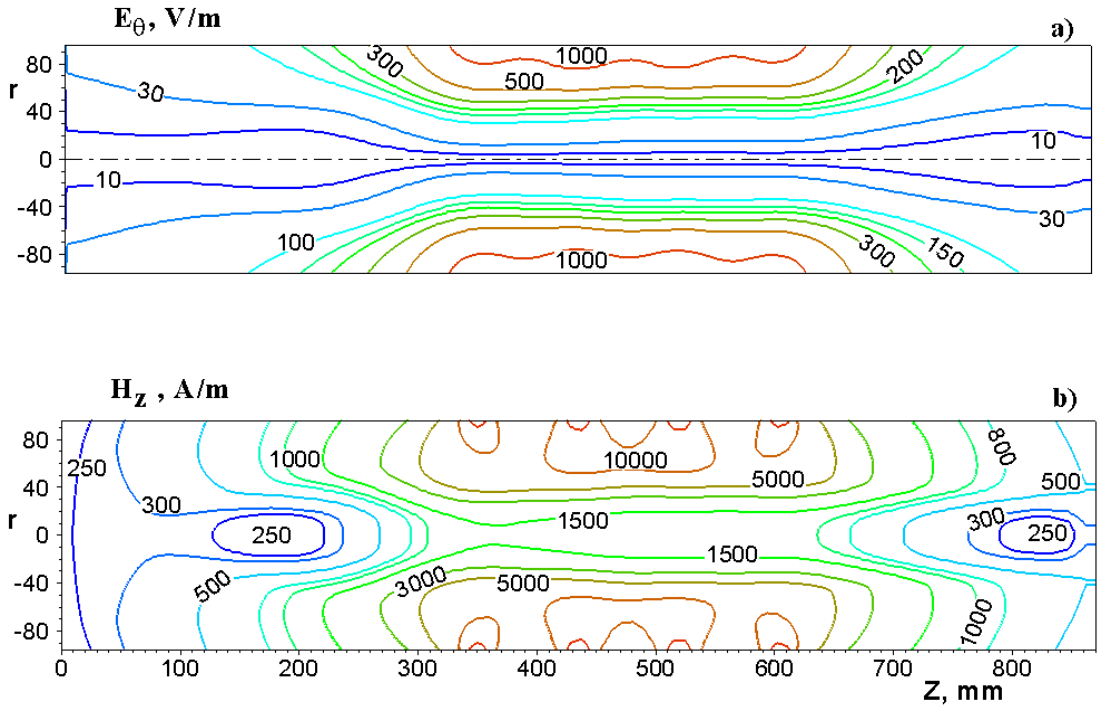


**Figure 8.** Contours of electric field (a) and magnetic field (b) amplitudes in IPG-3 channel, 2D model.

It is clear from the comparison of the corresponding figures 5 and 6, figures 7 and 8, that for IPG–3 plasmatron the difference between 1D and 2D results is much greater than for IPG-4 one. The

temperature maximums, the maximums of electric and magnetic field amplitudes obtained with 1D and 2D models are not very different, but the geometry of contours is essentially different.

To provide better quantitative comparison of the results obtained with use of 1D and 2D models, the radial profiles of air plasma velocity and temperature calculated at the exit section of IPG-4 discharge channel are presented in figures 9–10 for the 3 values of plasmatron power, obtained with use of 1D (blue circles) and 2D (black squares) models.

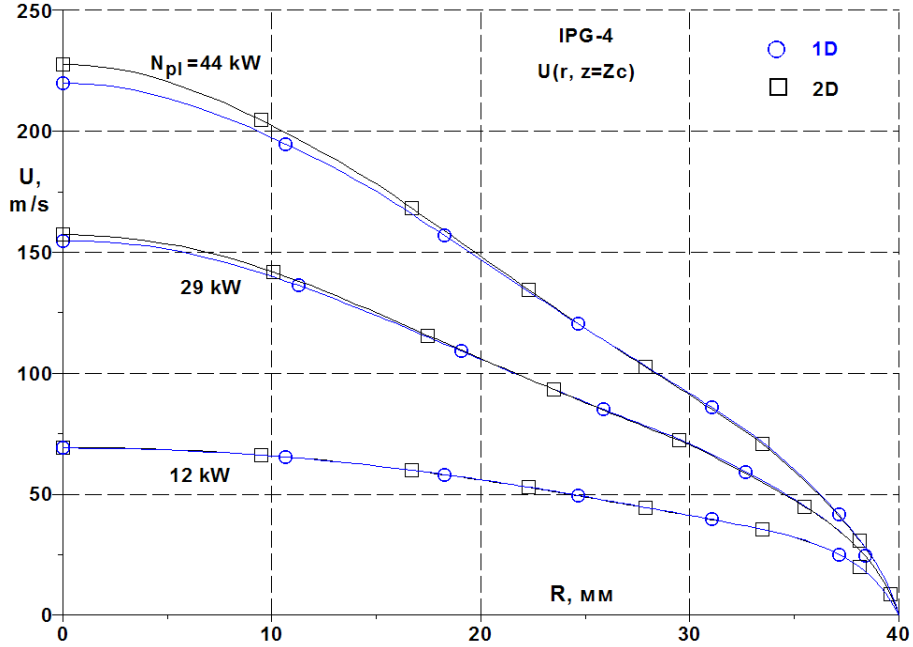


**Figure 9.** Radial profiles of plasma velocity at the IPG-4 channel exit section calculated with use of 1D and 2D models for 3 values of plasmatron power $N_{pl}$.

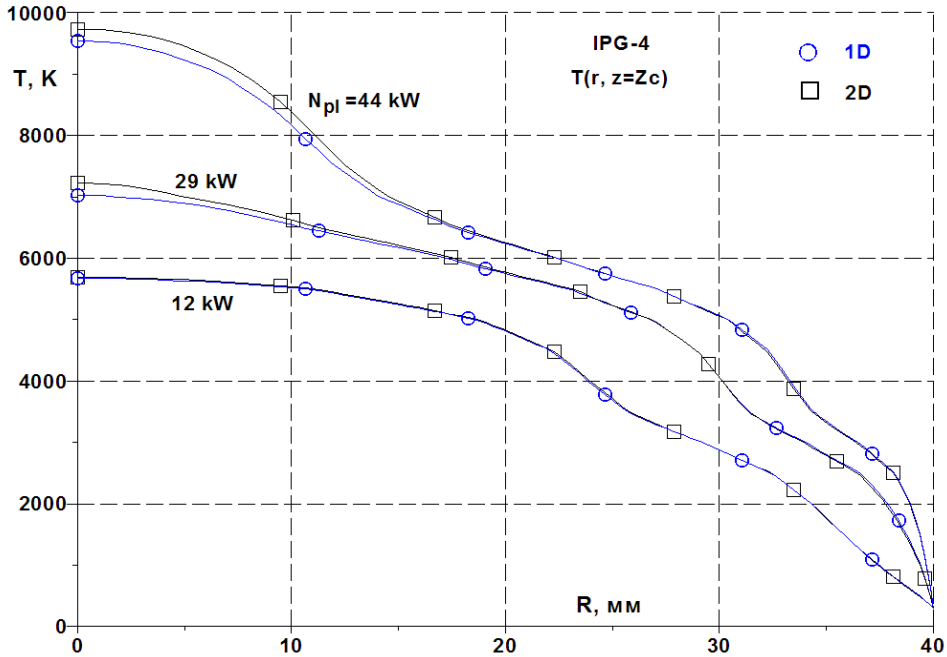


**Figure 10.** Radial profiles of plasma temperature at the IPG-4 channel exit section calculated with use of 1D and 2D models for 3 values of plasmatron power $N_{pl}$.

Similar radial profiles at the IPG-3 channel exit section are presented in figures 11-12.

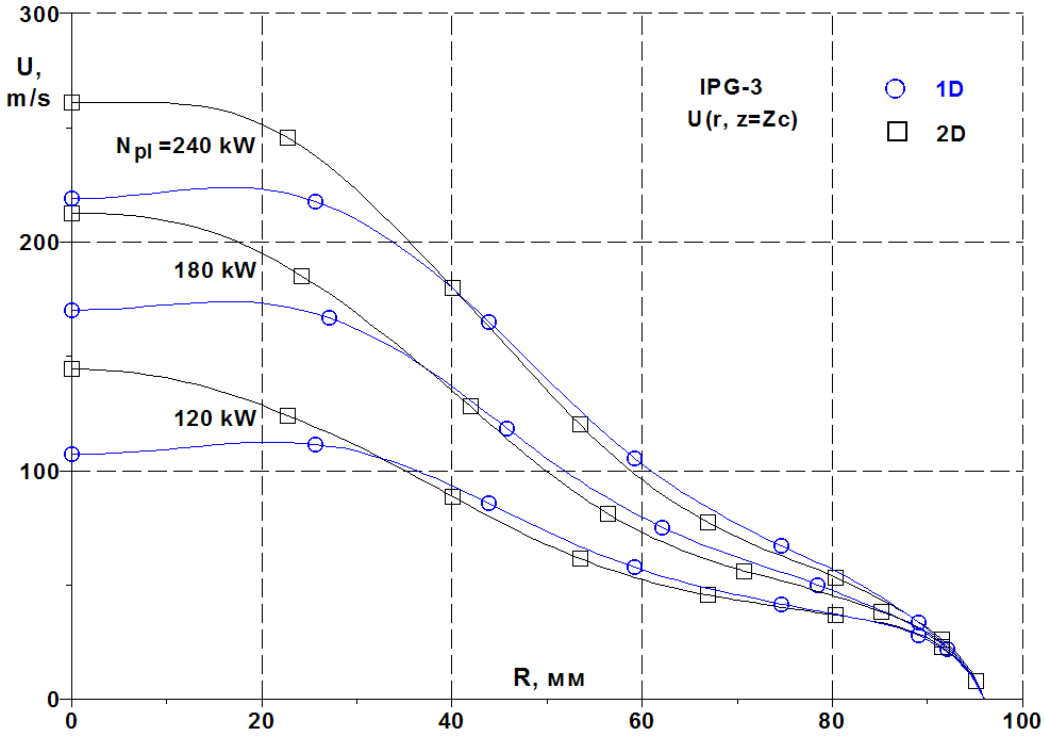


**Figure 11.** Radial profiles of plasma velocity at the IPG-3 channel exit section calculated with use of 1D and 2D models for 3 values of plasmatron power $N_{pl}$.

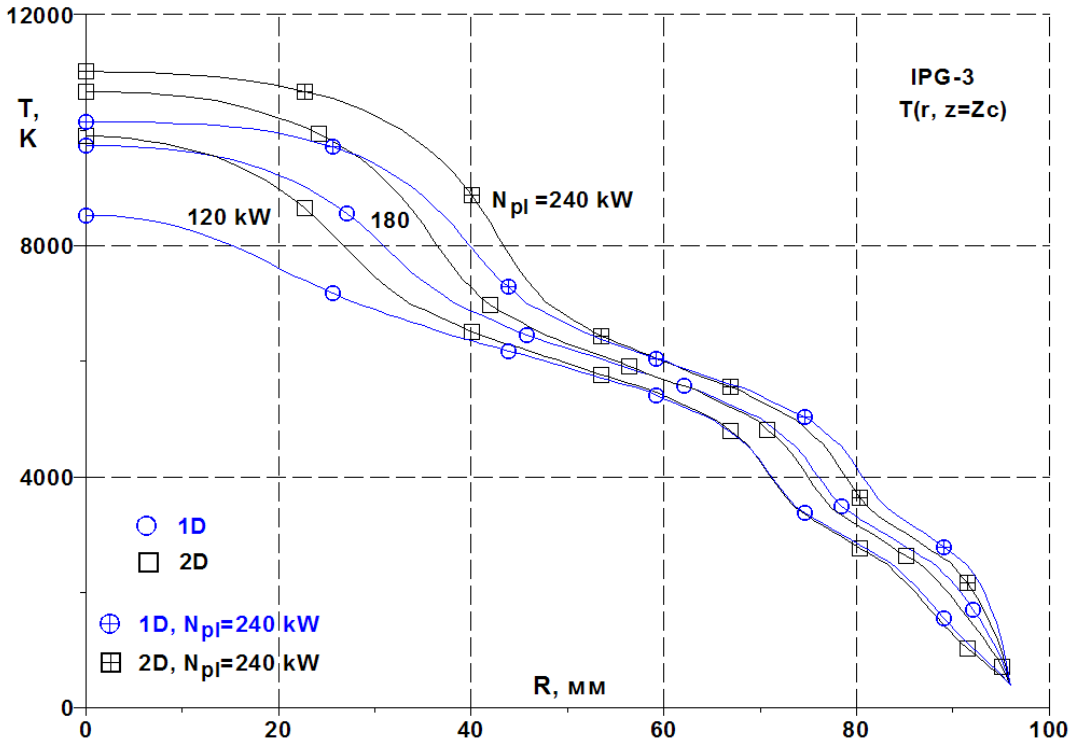


**Figure 12.** Radial profiles of plasma temperature at the IPG-3 channel exit section calculated with use of 1D and 2D models for 3 values of plasmatron power $N_{pl}$.

Figures 13–14 show the comparison of radial profiles of electric field amplitude $E_\theta$ at the middle of inductor region for IPG-4 and IPG-3, obtained with use of 1D and 2D models for 3 values of plasmatron power.

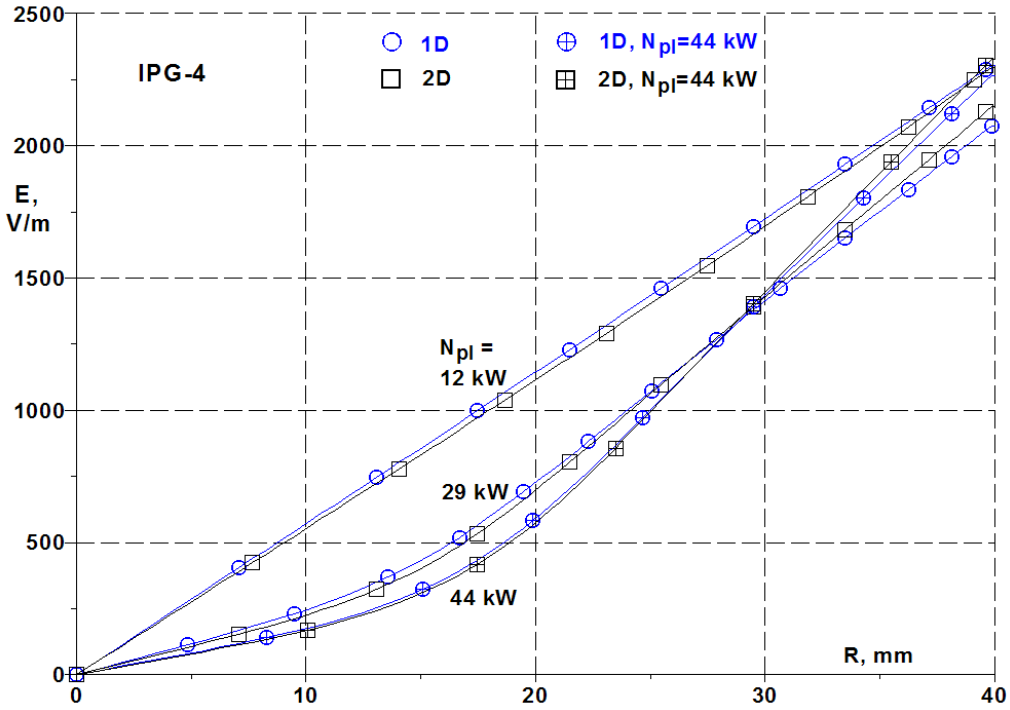


**Figure 13.** Radial profiles of electric field amplitude $E_\theta$ at the middle of inductor region for IPG-4, obtained with use of 1D and 2D models for 3 values of plasmatron power.

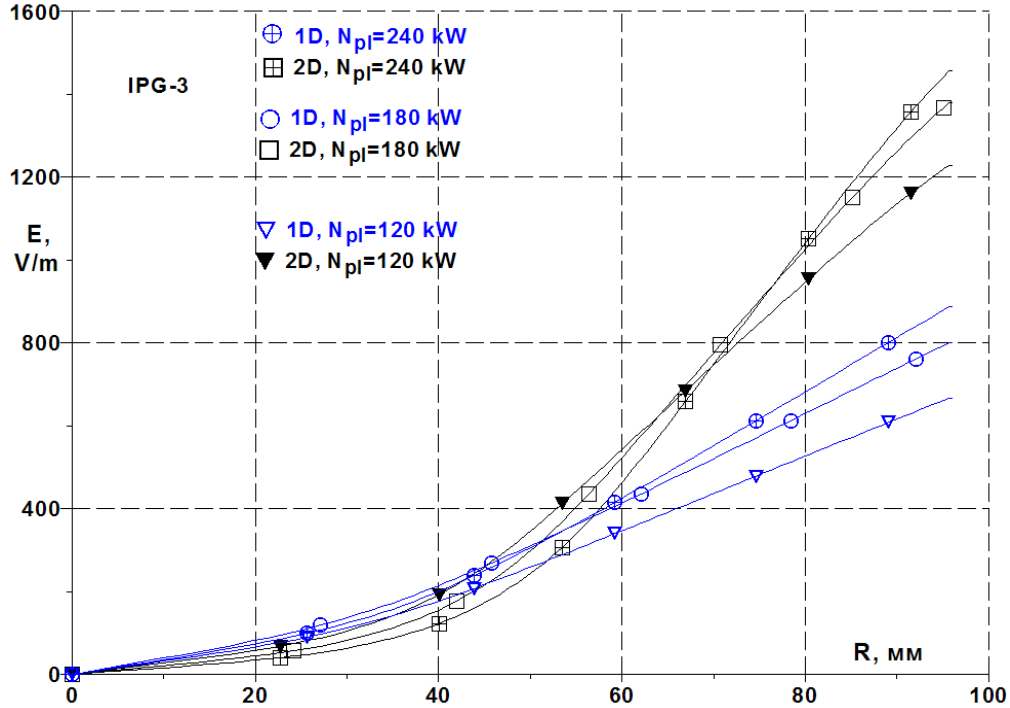


**Figure 14.** Radial profiles of electric field amplitude $E_\theta$ at the middle of inductor region for IPG-3, obtained with use of 1D and 2D models for 3 values of plasmatron power

Significant differences of 1D and 2D results are clear from figures 11, 12 and 14 for IPG-3 plasmatron, while for IPG-4 the corresponding differences are relatively small (figures 9, 10, 13).

Comparison of axial distributions of plasma velocity and temperature along the symmetry axis obtained by 1D and 2D models is presented in figures 15, 16 for IPG-4 plasmatron for the three values of plasmatron power. The similar results for IPG-3 plasmatron are presented in figures 17, 18.

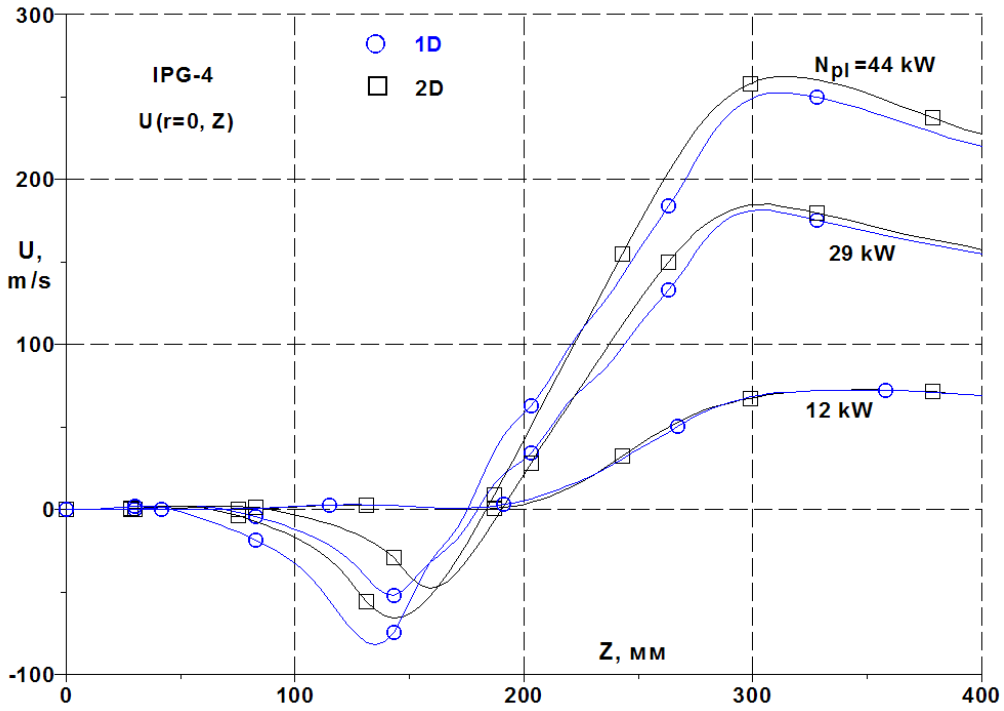


**Figure 15.** Axial distributions of plasma velocity along IPG-4 channel symmetry axis.

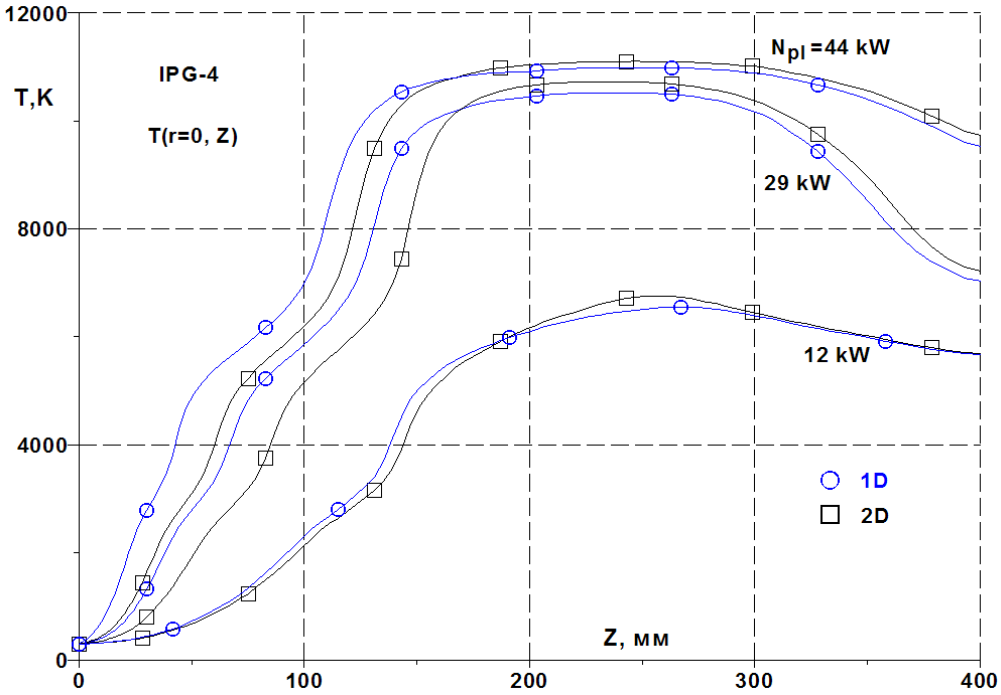


**Figure 16.** Axial distributions of plasma temperature along IPG-4 channel symmetry axis.

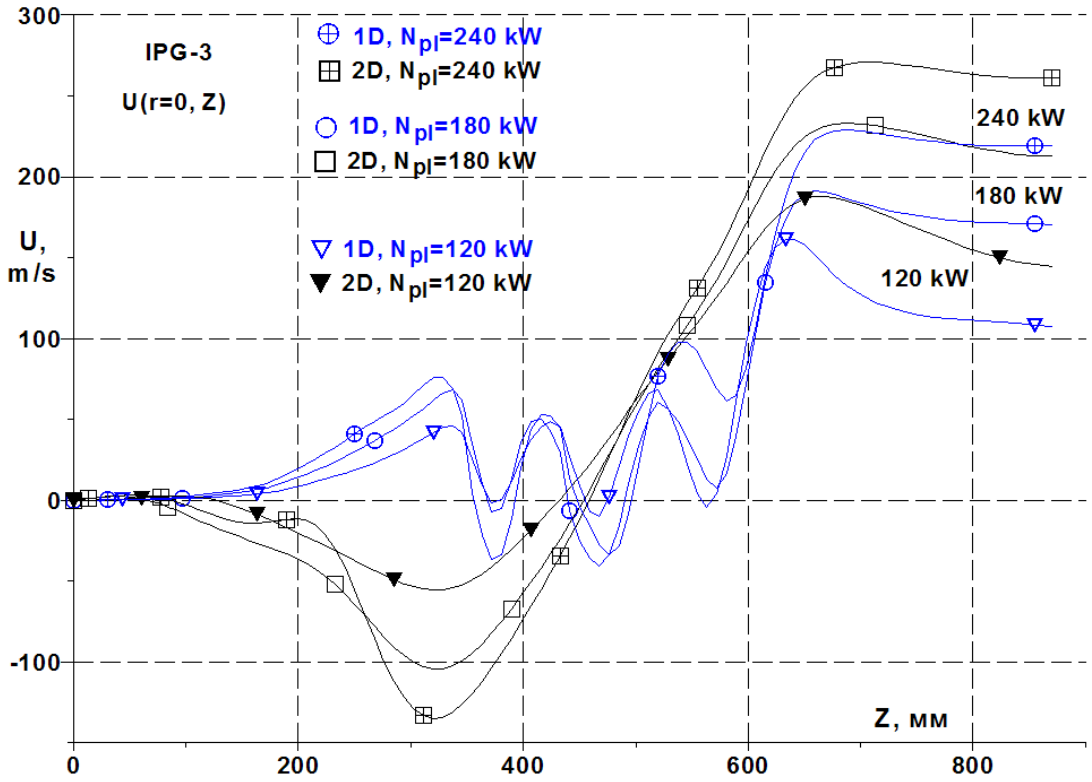


**Figure 17.** Axial distributions of plasma velocity along IPG-3 channel symmetry axis.

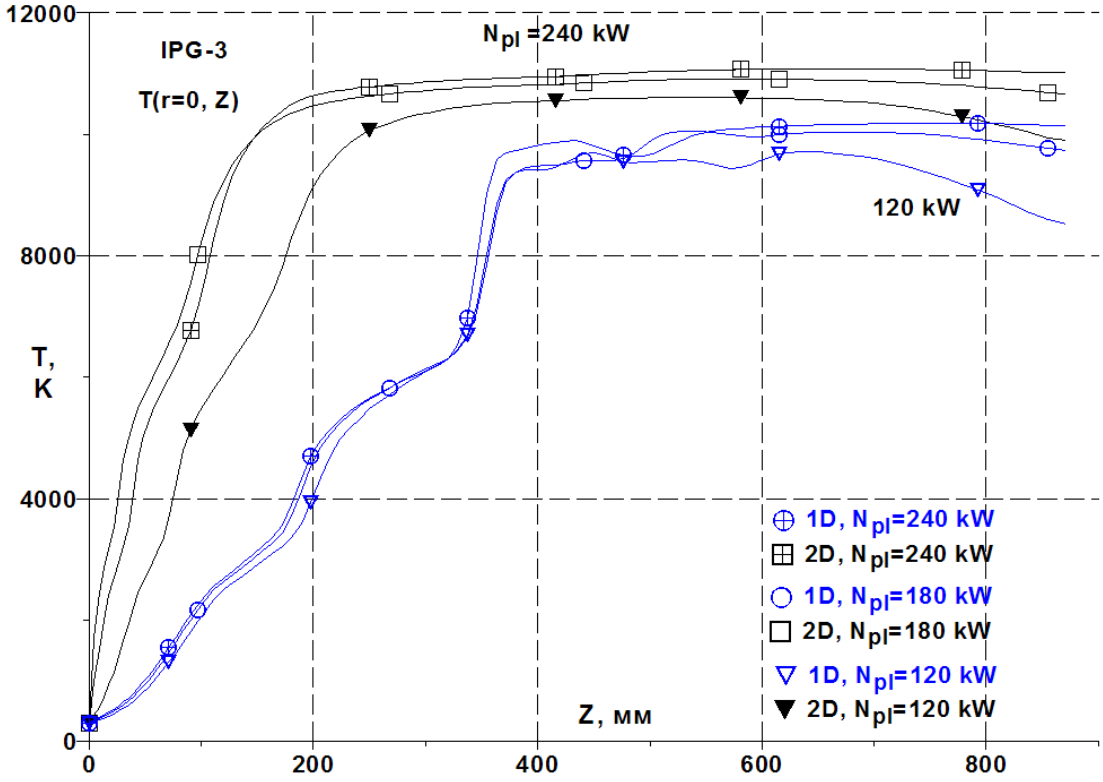


**Figure 18.** Axial distributions of plasma temperature along IPG-3 channel symmetry axis.

Again, essential differences of 1D and 2D results is clear from figures 17, 18 for IPG-3 plasmatron, while for IPG-4 the corresponding differences are relatively small (figures 15, 16).

Summing up the differences due to the use of 1D and 2D electromagnetic field models in flow parameters at the discharge channel exit section, important from practical viewpoint:

for IPG-4 plasmatron the differences in $U_c$ and $T_c$ between 1D and 2D results are very small for low power regime (0.4% and 0.3% for $U_c$ and $T_c$) and are relatively small for large power regime (4% and 2% for $U_c$, $T_c$), while for $h_c$ the difference is 2% - 3% for all regimes;

for IPG-3, 1D and 2D results are essentially different (up to 26%), and the differences in $U_c$ and $T_c$ are greater for low power regime (26% and 14% for $U_c$ and $T_c$), while for $h_c$ the difference is 17%÷18% for all regimes.

**Acknowledgements**
This work was partially supported by RFBR Grant No. 17-01-00054-a.

**References**

[1] Vlasov A V, Zalogin G N, Zemlyanskii B A and Knot'ko V B 2003 *Fluid Dynamics* **38** 815
[2] Gordeev A N, Kolesnikov A F and Yakushin M I 1992 *SAMPE Journal* **28** 29
[3] Vasil'evskii S A, Kolesnikov A F and Yakushin M I 1991 *High Temperature* **29** 411
[4] Vasil'evskii S A, Kolesnikov A F and Yakushin M I 1996 Mathematical models for plasma and gas flows in induction plasmatrons *Molecular Physics and Hypersonic Flows (NATO ASI Series* C vol 482) Ed M Capitely (Dordrecht: Kluwer) p 495
[5] Vasil'evskii S A and Kolesnikov A F 2000 *Fluid Dynamics* **35** 769
[6] Kolesnikov A F, Pershin I S, Vasil'evskii S A and Yakushin M I 2000 *The Journal of Spacecraft and Rockets* **37** 573
[7] Vanden Abeele D and Degrez G 2000 *AIAA Journal* **38** 234
[8] Boulos M I 1976 *IEEE Trans. on Plasma Sc*. **4** 28
[9] Vanden Abeele D, Vasil'evskii S A, Kolesnikov A F, Degrez G and Bottin B 1999 Code-to-code validation of inductive plasma computations *Progress in Plasma Processing of Materials* Ed P Fauchais and J Amouroux (New York: Begell House) p 245
[10] Bykova N G, Vasilevskii S A and Kolesnikov A F 2004 *High Temperature* **42** 12
[11] Ginzburg V L 1970 *The Propagation of Electromagnetic Waves in Plasmas* (Oxford, New York: Pergamon Press)
[12] Landau L D and Lifshitz E M 1963 *Electrodynamics of Continuous Media* (Oxford: Pergamon Press)
[13] Hirschfelder J O, Curtiss C F and Bird R B 1966 *Molecular Theory of Gases and Liquids* (New York: Wiley)
[14] Devoto R S 1966 *Physics of Fluids* **9** 1230
[15] Tirskii G A 1999 *Journal of Applied Mathematics and Mechanics* **63** 841
[16] Sokolova I A and Tirskiy G A 1997 Transport properties of gases and plasma mixtures for gas-dynamics simulation *AIAA Paper* 97-2584
[17] Patankar S 1980 *Numerical Heat Transfer and Fluid Flow* (New York: Hemisphere Publishing)
[18] Saad Y 2003 *Iterative Methods for Sparse Linear Systems (2nd edition)* (SIAM, Society for Industrial and Applied Mathematics)
[19] http://www-users.cs.umn.edu/~saad/software/SPARSKIT/